

# A rapid method for turbomachinery aerodynamic design and optimization using active subspace

## Original article

### Article history:

Submission date: 15 November 2023

Acceptance date: 18 February 2024

Publication date: 26 March 2024

This is the updated version of a paper originally presented at the Global Power and Propulsion Technical Conference, GPPS Hong Kong23, October 17-19, 2023.



### \*Correspondence:

FL: loufy@tsinghua.edu.cn

### Peer review:

Single blind

### Copyright:

© 2024 Xu and Lou © This is an open access article distributed under the Creative Commons Attribution Non Commercial License (CC BY-NC 4.0), which permits unrestricted use, distribution, and reproduction in any medium for noncommercial purposes only, provided the original work is properly cited and its authors credited.

### Keywords:

active subspace; turbomachines; aerodynamic design and optimization; dimension reduction

### Citation:

Xu J., Lou F. (2024). A rapid method for turbomachinery aerodynamic design and optimization using active subspace. *Journal of the Global Power and Propulsion Society*, 8: 24–38.  
<https://doi.org/10.33737/jgpps/184214>

Jiasen Xu<sup>1</sup>, Fangyuan Lou<sup>1,\*</sup>

<sup>1</sup>*Tsinghua University, Tsinghua Garden, Haidian District, Beijing 100084, China*

## Abstract

Preliminary design is a crucial step in the turbomachinery aerodynamic design process, which involves the initial conceptualization and serves as the foundation for subsequent detailed design and analysis. During preliminary design, designers typically use a combination of empirical correlations, simplified flow models, and computational tools to evaluate the impact of different design parameters on the machine's performance. This iterative process heavily relies on the designer's experience and knowledge, and errors made during preliminary design may not be rectifiable in later design phases. To address this challenge, this paper proposes a novel optimization strategy for turbomachinery aerodynamic preliminary design using active subspace. The method utilizes active subspace techniques to reduce the dimensionality of the design space, making efficient and accurate exploration of the space possible. In addition, the open-access *Multall* turbomachinery design suite is employed to evaluate the aero-thermal performance of different designs. The method was then utilized to optimize the aerodynamic design of the blade profile for a ducted fan. Results show that the optimization strategy can identify the most significant directions in the design space, providing designers with a clear path to achieving an optimal design. Overall, the proposed method can be of good value to the turbomachinery design community attribute to its reduced dependence on the designer's experience and elevated efficiency of the design process.

## Introduction

In recent years, with the development of aviation power systems, electric-driven distributed propulsion systems have become a research hotspot and have been applied to small and medium-sized aircraft (Yang et al., 2021). Compared to the traditional propulsion engine using fossil fuel, the all-electrical energy propulsion system has a great advantage in energy-using efficiency, operational cost, the environmental influence. In the thin-haul aviation operation, Dramatic reductions in energy costs are anticipated by Distributed Electric Propulsion (DEP) aircraft instead of aircraft with the conventional propulsion system by almost 84%. Moreover, the energy cost has cut operating costs by nearly 31% (Kim et al., 2018). Moreover, it also significantly increases the nose plane taking off and landing and the emissions of incomplete combustion products like CO<sub>2</sub>, SO<sub>2</sub>, NO<sub>2</sub>, and so on. A ducted fan driven by electricity is an important equipment for the electric propulsion system. Comparing standard rotors and propellers, ducted fans of the same size not only can produce stronger power and less noise (Wick et al., 2015), and its flow in the edge of blades is easier controlled (Perry et al., 2018),

but also make an aerodynamic structure more compact, improve the safety performance and lower noisy sound due to the ring effect of the duct (Li and Gao, 2005). It dramatically benefits the aircraft whole efficiency, capability, and flight stability.

The optimization of aerodynamic design of fan blades has been a topic of interest for several decades. In 1926, Mark et al. introduced a novel turbomachinery design system, T-AXI, which incorporated a duct fan blade geometry generator that allowed for the visualization and calculation of the aerodynamic characteristics of various blade components (Turner et al., 2010). Recently, Nsukka *et al.* proposed a simplified method for designing fan blade bases using conformal transformations based on the Zhukovsky transformation. Additionally, in 2019, Denton introduced the open-source turbomachinery aerodynamic design platform (*Multall*), which includes a meanline design module, blade geometry generator, and a 3D flow solver (Denton, 2017). To assess the fidelity of the *Multall* solver in simulating internal flow in low-speed turbomachinery, Piero et al. utilized the *Multall 18.3* software to predict the steady-state flow field in the annular sector of a 315 mm tubular axial fan (Danieli et al., 2021). The results indicated that the predicted pressure curve and the aerothermal efficiency tendency were in good agreement with experimental data, as well as with results from the state-of-the-art commercial software. Various optimization methods have been employed in the design of fan blades, leading to improved efficiency and performance. For instance, Cho used the gradient optimization method to design a ducted fan blade with the same efficiency but a 30% larger tip clearance (Cho et al., 2009). In general, most optimization methods rely on gradient or fuzzy positive correlation in search of an optimal design, and the curse of dimensionality remains a key problem. For turbomachines with tens of design parameters per blade row, numerous trials are required to search for an optimal design. Thus, adopting high-fidelity simulations in the optimization process for even a medium number of design parameters can be computationally expensive and time-consuming.

One emerging approach is the so-called “active subspace optimization method,” which identifies the primary direction in a design space, and quite promising progress was achieved in several gas-turbine-related applications. For instance, Ashley et al. established a subspace to design temperature probes with the goal to minimize hysteresis pressure loss and the ratio variation with Mach number. They obtained a relatively excellent temperature probe design (Scillitoe et al., 2020) by weighing the impact of design parameters on the design goal using linear combination weights. Additionally, Pranay used the active subspace method to reduce the dimensionality of a 25-dimensional fan blade design space to a 2-dimensional active subspace (Seshadri et al., 2018). They then created 2D contour maps to visualize the relationship between four target variables: cruise efficiency, cruise pressure ratio, maximum climb flow capacity, and sensitivity to fan manufacturing errors. Based on these maps, they recommended optimizing the blade design by exploring the high-dimensional design space. More recently, Wang et al. and Wei et al. applied the active subspace method to the uncertainty quantification (Wang et al., 2020, 2021) and design optimization (Wei et al., 2023) in turbulent combustion. The scope of the paper is to take a further step and develop a toolkit for rapid optimization of turbomachinery blade using the active subspace method and *Multall* turbomachinery design platform. Four main steps of the methodology involve the following:

1. Producing blade design data,
2. Constructing the active subspace in terms of adiabatic efficiency, mass flow, and pressure ratio,
3. Establishing optimization equations,
4. Solving the optimization problem and constructing a 3D model of the optimized turbomachinery blade.

## Results and discussion

---

A previously designed ducted fan for general aviation was selected to demonstrate the effectiveness of the proposed method. This section is oriented as follows: The first subsection describes the development of a Python-based numerical framework. This software platform allows one to model the performance of the ducted fan using numerical methods. Using Python, one can automate many of the calculations and explore the design space quickly. The second subsection defines the target design space. It involves specifying the range of values for each design parameter, such as reaction, flow coefficient, workload, fan diameter, etc., sampling over the design space of interest, and generating a set of candidate designs. The third subsection analyses sensitivity, including analysing how does the sample size affect active subspace dimensions or eigenvalues. The fourth subsection focuses on constructing and solving the optimization equation. It involves using mathematical techniques to construct an equation that relates the active subspace variables to the adiabatic efficiency of the ducted fan. One can then solve this equation to find the optimal values of the design variables that maximize adiabatic efficiency. The last subsection documents the results of the optimal aerodynamic design.

### Numerical framework

All the CFD results reported in this paper were obtained using the *Multall* turbomachinery design system in-house flow solver. The system comprises of three related programs developed using *FORTRAN77*: MEAGEN, STAGEN, and a 3D solver. MEAGEN performs a 1D calculation to obtain velocity triangles, set annulus boundaries, generate initial blade shapes, and twist them for a free/forced vortex design. The output file from MEAGEN serves as an input file for STAGEN, which defines the blade shapes. The 3D blade is generated by stacking and combining 2D blade shapes into stages. Finally, the *Multall* system reads the input file written by STAGEN and performs a 3D multistage calculation to predict the detailed flow pattern and overall performance. The roadmap of the design system is shown in Figure 1.

To automate the process, it would be beneficial to integrate the *Multall* turbomachinery design system within a Python-based blade optimization framework. One way to achieve this is by using function libraries, which are simple and cost-effective. Using a dynamic link library (DLL) instead of a static link library allows for repeated calls without wasting resources and can be changed without recompiling. Given the system’s structure, it is necessary to convert the three linked programs into DLLs, each corresponding to a specific aspect of the system. The main program can then call these DLLs in sequence, as shown in Figure 2. This approach enables more seamless integration of the *Multall* design suite with the Python-based optimization framework, making it easier for users to design and optimize turbomachinery blades.

### Target design space and sampling strategy

This section describes the exercise conducted on a single-stage ducted fan. It focuses on generating multiple blade-shape design samples using Gaussian random sampling. First, a design space of 16 parameters is established, listed in Table 1. The blade-shape design parameters serve as input parameters, while the three aero-thermal performance metrics are objectives to train the active subspace. This approach helps identify the most

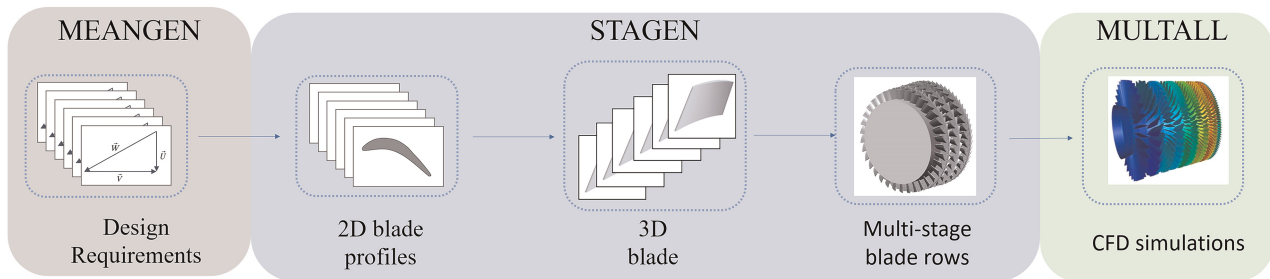


Figure 1. Roadmap of turbomachine aerodynamic design process using *Multall*.

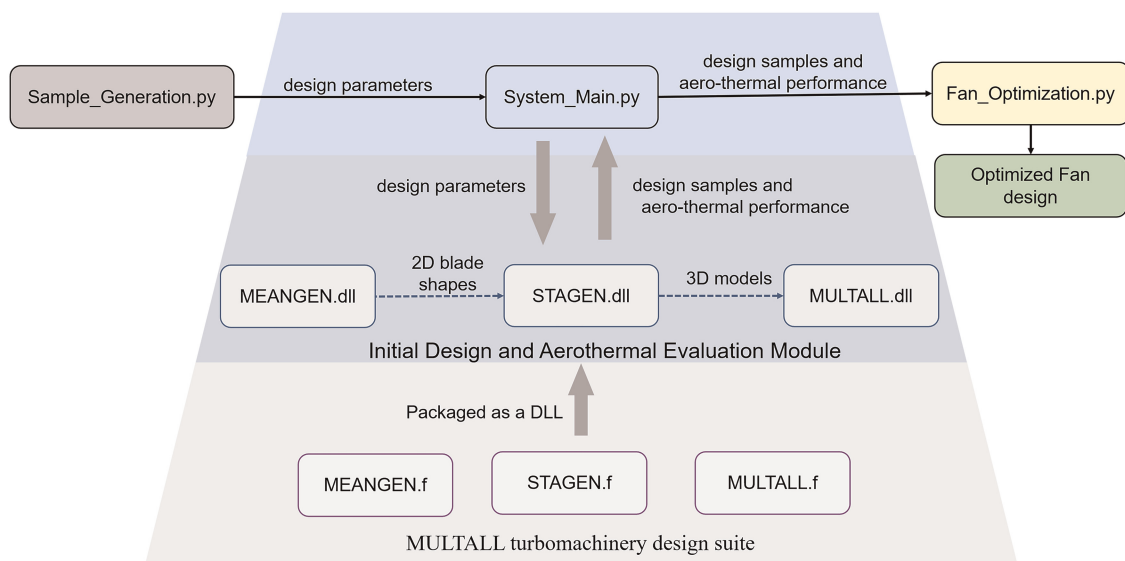


Figure 2. The Python-based blade optimization framework with integration of *Multall*.

Table 1. List of design parameters and sampling space.

No.	Parameter	Symbol	Nominal value	Lower limit	Upper limit	Unit
1	Reaction	$\Omega$	0.6	0.54	0.66	–
2	Flow coefficient	$\Phi$	0.7643	0.68787	0.84073	–
3	Loading coefficient	$\psi$	0.6269	0.56421	0.68959	–
4	Radius	$R$	0.325	0.2925	0.3575	M
5	Blade axial chord 1st row	$b_{ax\_1st}$	0.12	0.108	0.132	M
6	Blade axial chord 2nd row	$b_{ax\_2nd}$	0.1	0.09	0.11	M
7	Row gap	$G_{row}$	0.2	0.18	0.22	chord
8	Stage gap	$G_{stg}$	0.5	0.45	0.55	chord
9	First row deviation angle	$\delta_{1st\ row}$	6	3	9	deg
10	Second row deviation angle	$\delta_{2nd\ row}$	6	3	9	deg
11	First row incidence angle	$i_{1st\ row}$	–4	–2	–6	deg
12	Second row incidence angle	$i_{2nd\ row}$	–4	–2	–6	deg
13	First row LE QO angle	$S_{LE\ 1st\ row}$	88	84	92	deg
14	First row TE QO angle	$S_{TE\ 1st\ row}$	92	88	96	deg
15	Second row LE QO angle	$S_{LE\ 2nd\ row}$	92	88	96	deg
16	Second row TE QO angle	$S_{TE\ 2nd\ row}$	88	84	92	deg

critical input parameters that impact the performance metrics most, allowing for more efficient optimization of blade designs.

The design parameters are defined around normal values and sampled using Gaussian random sampling with  $N = 344$ . The range of each parameter is listed in Table 1. Each sample set  $\hat{x}_j$  is a vector of 16 dimensions and the value of each element falls within the range  $[x_l, x_u]$ , its description is:

$$\hat{x}_j = N(\mu, \sigma^2) \tag{1}$$

$\hat{x}_j$  represents the vector of  $j$ th samples of input parameters.  $\mu$  is a  $m$ -vector and equal to the average of  $x_l$  and  $x_u$ , shown in Equation (3). According to sigma rules,  $\sigma$  is defined:

$$\sigma = \frac{x_u - \mu}{3} \tag{2}$$

$$\mu = \frac{x_u + x_l}{2} \tag{3}$$

As to the sample size requirement, the size of samples must be larger or equal to  $G = \alpha k(m + 1) \ln(m)$ . An oversampling factor,  $\alpha$ , between 2 and 10 is typically selected in practical applications. This ensures that the sample is large enough to capture the variability in the data and provide statistically significant results. Lastly, a normalization process is employed to ensure that the analysis is not affected disproportionately by parameters with larger values. The normalization process involves transforming the input parameter vector  $\hat{x}_j$  of each sample to a standard range. This standard range centers all the transformed parameters at zero, making them dimensionless and giving them equal weight in the analysis. The standard range of the transformed parameters is  $[-1, 1]^m$ , where  $m$  is dimension of the design space. The normalization is carried out using Equation (4).

$$x_j = \frac{1}{2}(\text{diag}(x_u - x_l)\hat{x}_j + (x_u + x_l)) \tag{4}$$

### Active subspace identification

This study carried out active subspaces for three critical aero-thermal parameters of the ducted fan. The first objective is to optimize the adiabatic efficiency of the single-stage fan, which is the primary focus of the study. The second objective is the flow capacity of the fan, which is restricted in this study. The third objective is to ensure that the pressure ratio of the fan is equal to the pressure ratio of the baseline design.

### In term of adiabatic efficiency

An active subspace for adiabatic efficiency is sought to capture its variation in 16-dimensional space with fewer dimensions. The goal is to construct an active subspace that reduces the dimensionality to the expected dimension, which is determined by evaluating the gap in the eigenvalues (Constantine, 2015).

The first step is to calculate the subspace eigenvalues of each dimension using gradient decomposition. If gradients are not available, finite difference approximations can be used to obtain approximate values of the gradient. In this study, the small design space makes it feasible to use finite difference approximations. eigenvalues  $\lambda_k$  and corresponding eigenvectors  $\eta_k$  are obtained for each dimension  $k = 1, \dots, 16$ . The eigenvalues are then plotted on a log scale, as shown in Figure 3. Figure 3(a) shows that the largest gap lies between the 1st and 2nd index, indicating that the most suitable active subspace is one in this case. Figure 3(b) plots the estimated eigenvalues along with the bootstrap intervals and shows that the calculation error in the scenario of a single dimension is the smallest.

The main idea behind subspace dimensionality reduction is to use matrix multiplication between the input parameter vector and a tall transformed matrix, reducing the high dimensionality of  $m$  to a lower dimensional  $s$ . The transform  $z_j = M^T x_j$  is called a forward map, where  $z_j \in R^s$ ,  $x_j \in R^m$ ,  $M \in R^{m \times s}$ . It maps the  $m$ -dimensional design vector to an  $s$ -dimension coordinate. The transform matrix is determined by the eigenvalues and eigenvectors, and a large gap between the  $s$ th and  $(s + 1)$ th eigenvalue indicates a strong univariate trend between the objective  $y_i$  and the combined matrix of the first  $s$  eigenvectors,  $M = (\eta_1, \eta_2, \dots, \eta_s)^T x_j$  (Constantine, 2015). In this study, the first eigenvalue was found to have the largest gap, indicating that the transform matrix  $M_1$  for the efficiency active subspace is a matrix stacked with the first eigenvector. This matrix

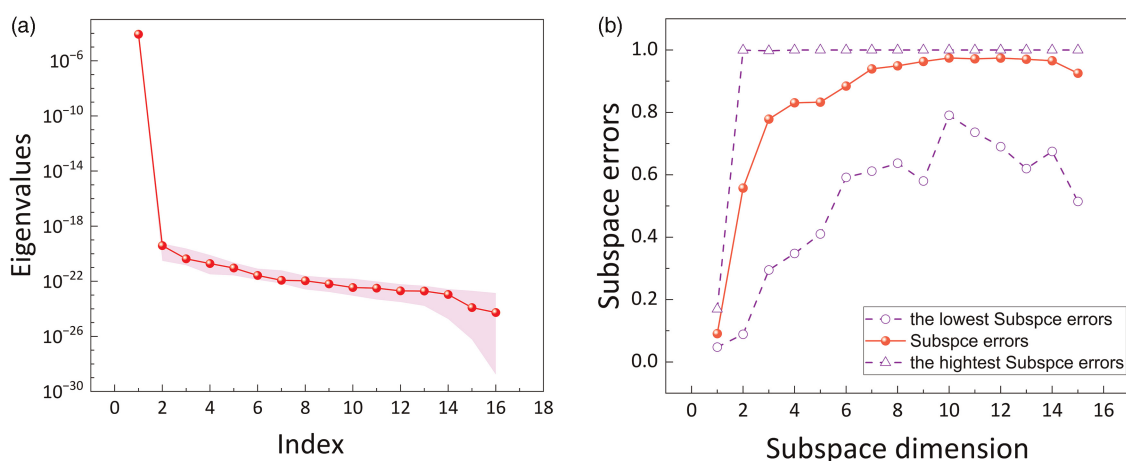


Figure 3. The eigenvalues (a) and subspace errors (b) of adiabatic efficiency active subspace.

is described:

$$M_1 = (0.431, -0.091, 0.188, 0.783, -0.071, -0.007, -0.013, -0.001, -0.288, -0.075, -0.164, -0.146, -0.111, 0.199, 0.484, -0.001)^T \tag{5}$$

Furthermore, Figure 4 shows the relationship between the forward map  $z$  and the adiabatic efficiency  $\gamma_1$ . The figure depicts a manifold relationship between the map of 16 design parameters and adiabatic efficiency  $\gamma_1$ , indicating that the most significant direction of the design parameters space, along which the largest change of the adiabatic efficiency occurs, has been successfully identified. As shown in the figure, adiabatic efficiency varies as a quadratic function curve along a single vector in the 16-dimensional design space. This confirms that the active subspace has reduced the high-dimensional design space to a lower dimensional space capturing the most significant variations in the objective.

### In term of mass flow rate

Following the same procedure, the active subspace for mass flow is identified. Same as the adiabatic efficiency, the largest gap between adjacent eigenvalues in the scenario of mass flow also lies between the 1st and 2nd index, shown in Figure 5(a). Additionally, a single dimension also yields the smallest error, shown in Figure 5(b). Lastly, the transform matrix,  $M_2$ , is obtained. The scatter plot, Figure 5(c), indicates a fairly linear connection

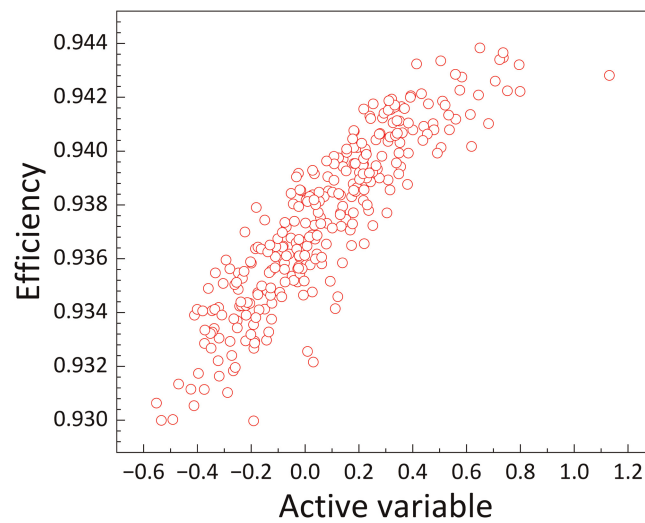


Figure 4. Scatters of adiabatic efficiency in efficiency active subspace.

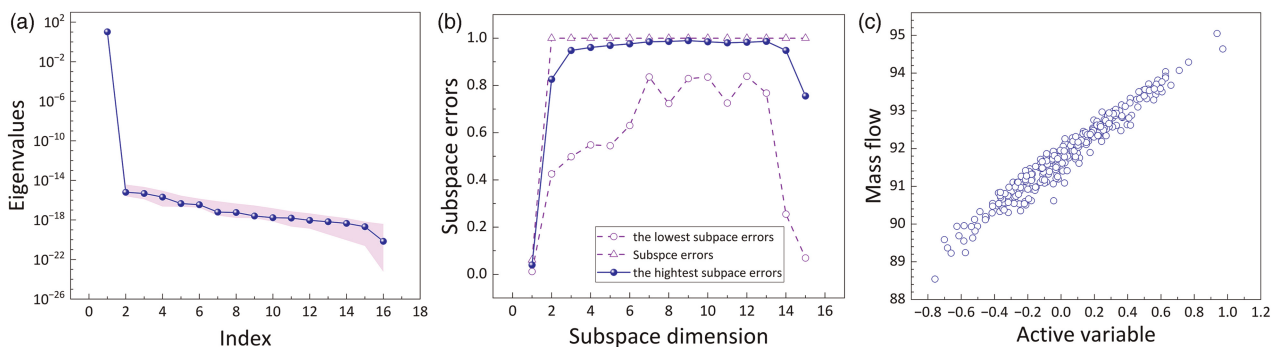


Figure 5. The eigenvalues (a), subspace errors (b) and scatters of mass flow (c) in mass flow active subspace.

between the subspace  $M_2^T x$  and mass flow  $y_2$ .

$$M_2 = (0.036, 0.272, -0.165, 0.293, -0.018, -0.008, 0.017, 0.08, 0.845, 0.102, -0.253, -0.126, -0.109, -0.059, -0.003, -0.047)^T \tag{6}$$

**In term of pressure ratio**

Lastly, the active subspace for the total-to-total pressure ratio is identified. Similarly, the largest gap between adjacent eigenvalues in the scenario of total-to-total pressure ratio also lies between the 1st and 2nd index, shown in Figure 6(a), and a single dimension yields the smallest error, shown in Figure 6(b). Lastly, a linear connection between the subspace  $M_3^T x$  and mass flow  $y_3$  was spotted, shown in Figure 6(c).

$$M_3 = (2.55e^{-2}, -6.22e^{-4}, -4.41e^{-1}, -8.84e^{-1}, 8.57e^{-4}, -1.01e^{-3}, 1.57e^{-3}, -3.92e^{-4}, -1.47e^{-1}, 1.05e^{-2}, 4.29e^{-2}, 8.02e^{-3}, 4.29e^{-3}, 1.44e^{-2}, -9.69e^{-4}, 7.41e^{-3})^T \tag{7}$$

To summarize, this section discusses the use of active subspaces to identify dominant directions in a high-dimensional design space. By using this technique, the authors were able to reduce the dimensionality of the design space and identify the most significant design parameters affecting the performance of a ducted fan. Results show that active subspace exists for fan adiabatic efficiency, mass flow rate, and total-to-total pressure, and the most suitable dimension for all three parameters is one. For adiabatic efficiency, a manifold relationship between the subspace and adiabatic efficiency is observed, where the adiabatic efficiency varies as a quadratic function curve along a single vector in the 16-dimensional design space. A fairly linear connection between the subspace and the parameter is concluded for mass flow and total-to-total pressure ratio.

**Fidelity analysis**

Despite the promising result presented in the above section, questions remain such as independence of the active subspaces, sensitivity of parameters, and accuracy of manifold modelling. This section investigates the fidelity of the active subspace approach. First, to verify the independence of the previously identified active subspaces, additional data samples can be generated randomly in the design space and used to compute the subspaces again. If the resulting subspaces are similar to those computed earlier using the limited number of samples, it can be concluded that the subspaces are independent of the specific data samples used and represent the dominant direction of the objective in the whole design space. To investigate the sensitivity of various design parameters, the gradient of the objective function for each design parameter can be calculated using the active subspace. This will provide insight into which design parameters impact the objective most and can be used to guide the optimization process. Lastly, a manifold model can be fitted to the data in the active subspace, which can be done using linear regression for a linear model or polynomial regression for a quadratic model. The accuracy and fitness of the model can be evaluated using statistical metrics such as the R-squared value and mean squared error.

**Independence of active subspace**

Two questions need to be addressed to verify the independence of the active subspaces from the data samples. The first question is whether the active subspaces would differ with different sample contents for the same

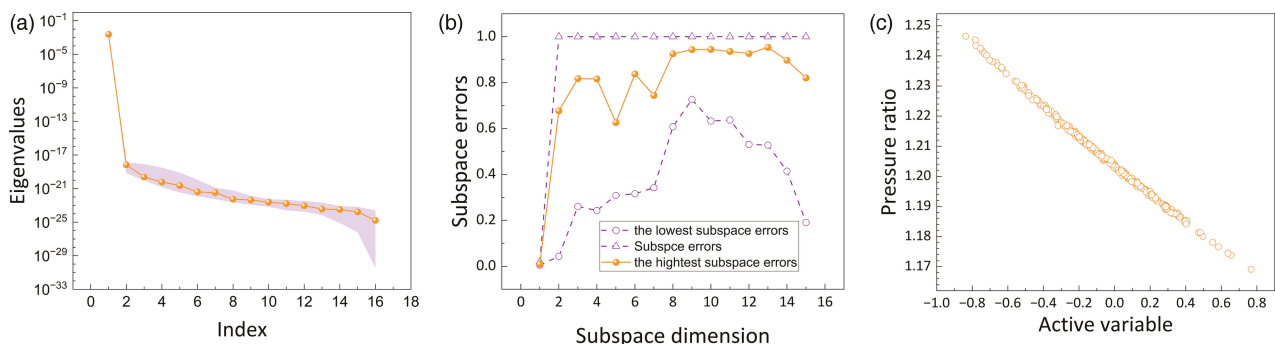


Figure 6. The eigenvalues (a), subspace errors (b) and scatters of pressure ratio (c) in pressure ratio active subspace.

sample size, and the second question is whether the sample size can affect the result of the active subspaces. This section uses a series of samples of different sample counts to investigate the effect of the sample size on the active subspaces. The recommended sample size  $G = \alpha k(m + 1)In(m)$  is used to set the upper and lower bounds for the smallest sample size for finding a functional subspace. The constant  $\alpha$  is an oversampling factor typically chosen to be between 2 and 10. Gaussian random sampling is used to select numerous data samples from the design space, with sample sizes ranging from 100 to 500 with an interval of 50. These samples are used to perform simulations and obtain the objective metrics for finding the active subspaces. The results for the adiabatic efficiency subspace are shown in Figure 7. There is little difference in the eigenvalues for sample size varying from 100 to 500, shown in Figure 7(a). The subspace error and eigenvector components also change within the permissible error range, as shown in Figures 7(b) and 7(c).

Additionally, the independence of the mass flow rate subspace is also shown in Figure 8. Figures 8(a) and 8(b) demonstrate no significant difference in the existing eigenvalues and subspace errors for each dimension among different sample sizes. The subspace components also fluctuate only slightly within a very small range. Lastly, Figure 9 shows that the pressure ratio subspace is almost unaffected by the training samples, as the curve remains the same as the sample size increases. These results demonstrate that the active subspaces discussed in Section 2.3 are independent of the data samples used in the calculation process.

### Sensitivity analysis in terms of parameters

In Section 2.4.1, it is demonstrated that the elements of transformed matrices  $M$  are independent of the size and content of the samples used in the calculation process. These matrices are used to transfer the 16D design space to a 1D space, with aero-thermal performances serving as the objective metric. This means that the active subspaces are also a combination of all design parameters, with coefficients linking each parameter to the significance of the objective. A larger coefficient indicates that the objective value is more sensitive to changes in the related parameter. Figure 10 plots the eigenvector components of each active subspace and the component weights of all design parameters. In Figure 10(a), the adiabatic efficiency active subspace has 16 components associated with the 16 design parameters. The height of each column in each index corresponds to the influence of the

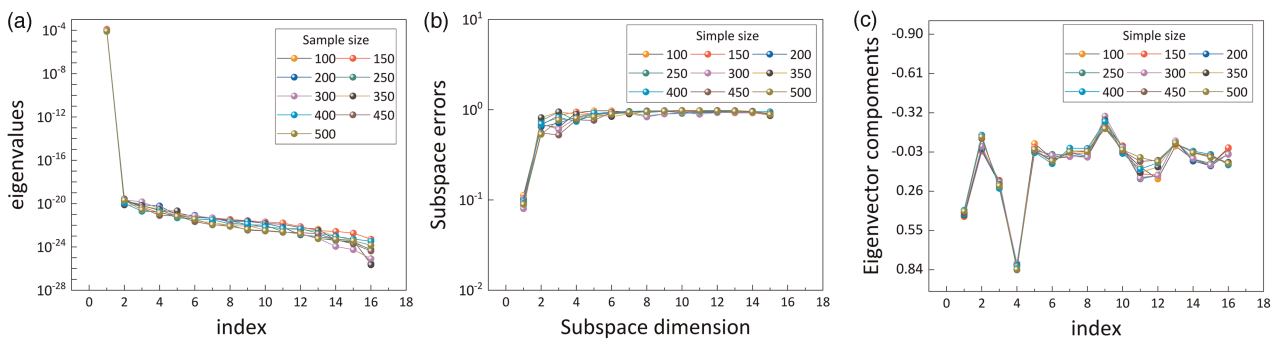


Figure 7. The independence verification for adiabatic efficiency subspace: eigenvalues (a), subspace errors (b) and eigenvector components (c).

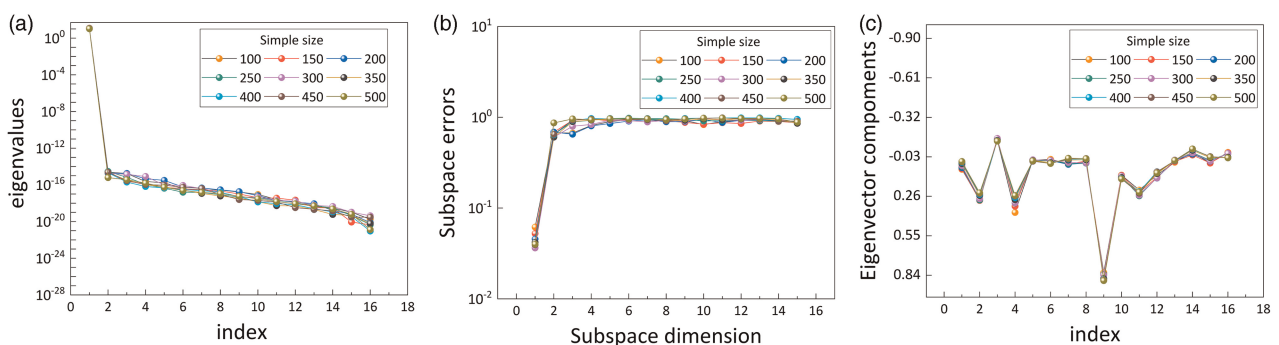


Figure 8. The independence verification for mass flow subspace: eigenvalues (a), subspace errors (b) and eigenvector components (c).

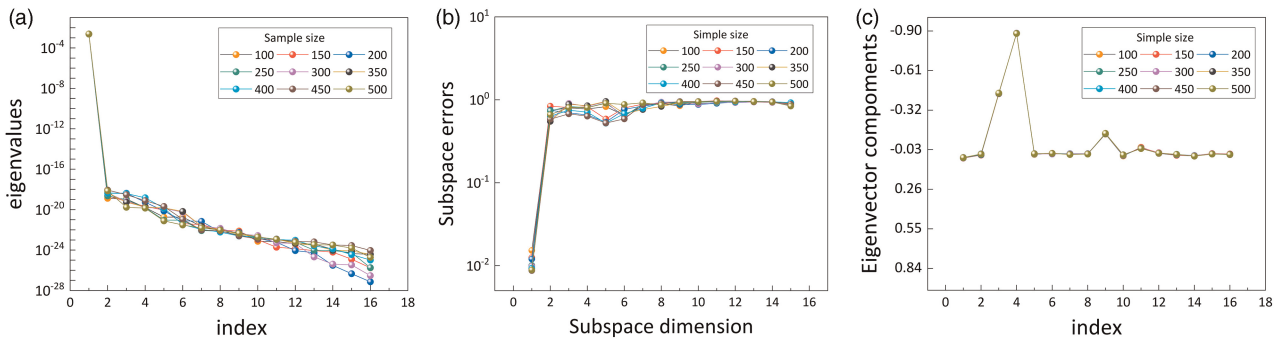


Figure 9. The independence verification for pressure ratio subspace: eigenvalues (a), subspace errors (b) and eigenvector components (c).

parameters on adiabatic efficiency. The largest perturbation is caused by Radius, followed by Reaction, First-row deviation angle, and so on. Figure 10(b) shows the distribution of elements for vector  $M_2$ , which represents the contribution to the dominant direction. This figure shows that design variables such as First-row deviation angle, Radius, and Flow Coefficient have greater weights in the direction. In contrast, Second-row LE QO angle, Blade Axial Chord 2nd row, and Stage Gap have less influence. Lastly, Figure 10(c) indicates the significance of the components corresponding to  $M_3$  in the active subspace. Increasing the pressure ratio is mainly achieved through changes in the Radius and Loading Coefficient, with the remaining design variables contributing less to this objective. Overall, these findings highlight the important role that each design parameter plays in determining the overall performance of the ducted fan, as well as the usefulness of the active subspace methodology in identifying the most critical parameters.

Fitting curve of active subspace

This section uses polynomial fitting to build fitting curves in the active subspaces. Polynomial fitting aims to establish a functional relationship between the map  $z = M^T x$  and the objective  $y$  using a polynomial with degree  $n$ .

$$y = a_0 + a_1z + a_2z^2 + \dots + a_nz^n \tag{8}$$

where  $n$  can be any positive integer.

The scatter plots in Figures 4(a), 5(c), and 6(c) show the distribution of design samples in each active subspace. Based on these scatter plots, linear or quadratic responses may fit the trend of the scatter distribution very well. Therefore, using first-order polynomial and secondary-order polynomial to fit the objectives  $y_1, y_2, y_3$  in their subspaces.

$$y = a_0 + a_1z \tag{9}$$

$$y = a_0 + a_1z + a_2z^2 \tag{10}$$

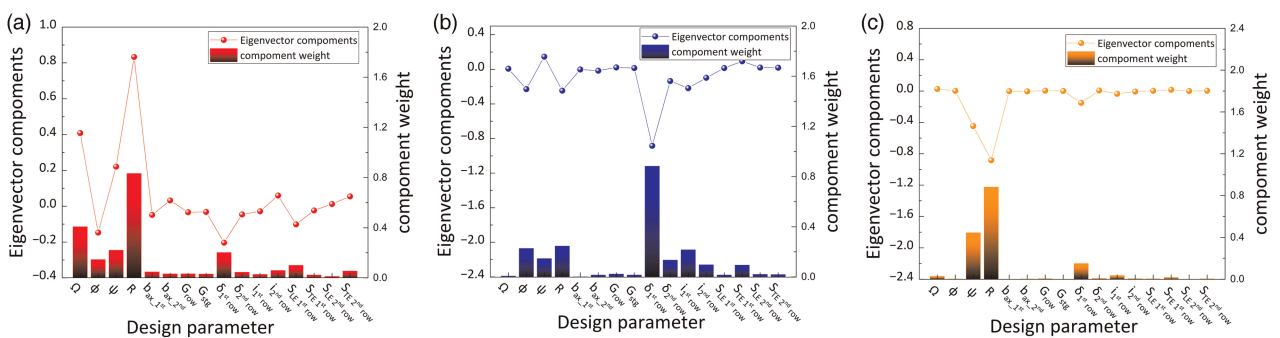


Figure 10. The eigenvector components and corresponding weight of design parameters: efficiency active subspace (a), mass flow active subspace (b), pressure ratio subspace (c).

To compute the coefficients associated with the models, Equations (9) and (10) are built using samples. To choose the best function curve fitting the plots, the correlation coefficients of the two functions in all active subspaces must be compared. Figure 11(a) compares the correlation coefficients of the first-order and second-order polynomials with different sample sizes in the efficiency subspace. The graph shows that the line of the second-order polynomial fitting is above that of the first-order polynomial from beginning to end, indicating that the quadratic curve has a stronger correction of sample scatters in the efficiency subspace. Furthermore, the quadratic curve tends to be stable, and the coefficients in the line still drop as the sample size increases. Thus, the second-order polynomial fitting is chosen, and the related coefficients are computed using Equation (11).

$$f_1 = 0.937 + 0.0104z_1 - 0.00433z_1^2 \tag{11}$$

where  $f_1$  is the proper function of efficiency active subspace based on 300 training samples. The coefficient  $R_1^2$  is 0.873. The polygonal lines in Figures 11(b) and 11(c) show a small distance, and fitting curves of different sample sizes all share high coefficients. Considering calculation convenience and the light influence of the two constraint objectives to optimize blade efficiency, mass flow and pressure ratio active subspaces use first-order polynomial fitting, shown in Equations (12) and (13).

$$f_2 = 91.739 + 3.333z_2 \tag{12}$$

$$f_3 = 1.204 - 0.0491z_3 \tag{13}$$

where  $f_2$  and  $f_3$  are the appropriate functions of mass flow and pressure ratio active subspaces, respectively, both calculated using 300 samples. Their coefficient  $R_2^2$  and  $R_3^2$  are 0.972 and 0.998, separately. Finally, the fitting curves with sample scatters are displayed in Figure 12.

### Optimization of a single-stage fan blade

This section focuses on optimizing a single-stage fan blade with specific parameters shown in Table 1. Using the *Multall* solver, the adiabatic efficiency, mass flow, and pressure ratio of the fan are computed as 93.401%,

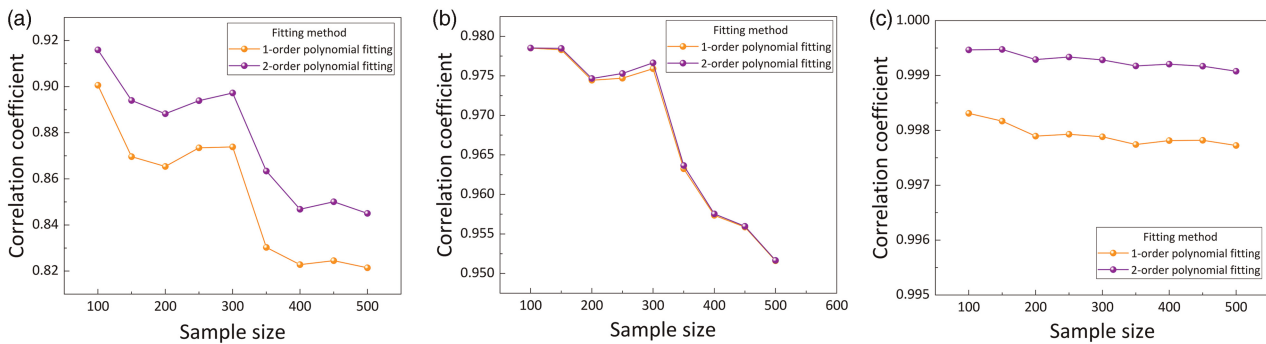


Figure 11. Correlation coefficients of two fitting curves in different sample size: adiabatic efficiency (a), mass flow (b) and pressure ratio (c).

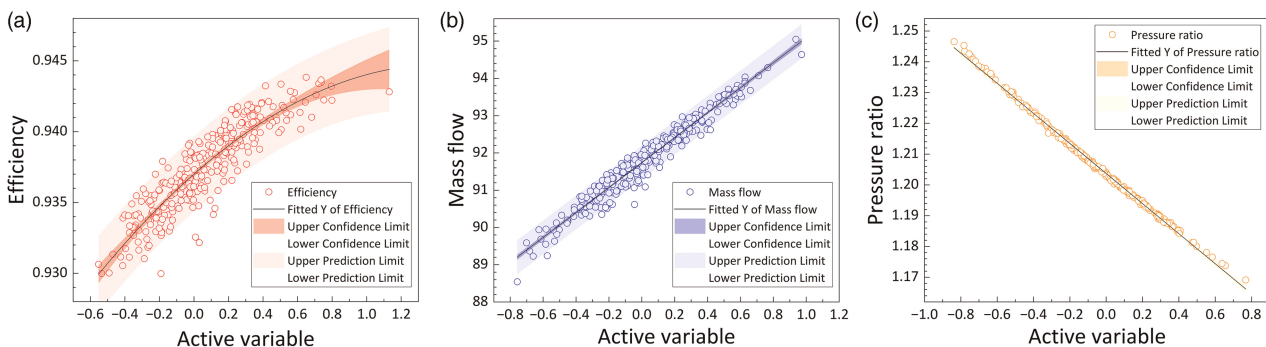


Figure 12. Fitting curves in active subspace: adiabatic efficiency (a), mass flow (b) and pressure ratio (c).

92.022 kg/s, and 1.202, respectively. The main objective of the optimization is to maximize the adiabatic efficiency while keeping the mass flow and pressure ratio constant. An equation group that includes constraint equations from the mass flow and pressure ratio active spaces and an objective equation from the efficiency space is constructed to achieve this objective. The equation assembly is presented in Equation (14).

$$\begin{aligned} \max \quad & 0.937 + 0.0104z_1 - 0.00433z_1^2 \\ & \begin{cases} 91.739 + 3.333z_2 = 92.022 \\ 1.204 - 0.0491z_3 = 1.2022 \\ z_1 = M_1x \\ z_2 = M_2x \\ z_3 = M_3x \\ x_{\min} \leq x \leq x_{\max} \end{cases} \end{aligned} \tag{14}$$

Prior to solving the above equation assembly, it is important to analyze the monotonicity of the objective function with respect to the constraints. By examining the plot of the quadratic function, it is evident that the objective function first increases and then decreases at the axis of symmetry  $-b/2a = 1.205$ . Therefore, it is necessary to get the value range of  $z_1$ , the other maximizing problem shown in Equation (15).

$$\begin{aligned} \max \quad & z_1 = M_1x \\ & \begin{cases} M_2x = 0.084995 \\ M_2x = 0.035272509 \\ x_{\min} \leq x \leq x_{\max} \end{cases} \end{aligned} \tag{15}$$

This optimization problem is solved using the simplex algorithm, and the resulting design vector  $x'_{\max}$  is shown in Equation (16), which corresponds to the maximum value of  $z_1$ . As the maximum value of  $z_1$  is 1.567, which is greater than the axis of symmetry at 1.205, it can be concluded that the maximum efficiency of 94.337% is achieved when  $z_1 = 1.205$ .

$$x'_{\max} = (6.6, 0.689, 0.564, 0.34, 0.108, 0.11, 0.18, 0.45, 5.572, 9, -2, -2, 84, 88, 96, 92)^T \tag{16}$$

Furthermore, Equation (14) can be transformed as a group of indefinite equations, shown in Equation (17).

$$\begin{aligned} & \begin{cases} M_1x = 1.20471 \\ M_2x = 0.084995 \\ M_2x = 0.035272509 \\ x_{\min} \leq x \leq x_{\max} \end{cases} \end{aligned} \tag{17}$$

Since three equations can only solve for three unknowns, the three most sensitive parameters – radius, first-row deviation angle, and loading coefficient – are selected as unknowns in Equation (17). The other parameters are considered as known values obtained by average random sampling in the design space. However, it was found that Equation (17) was difficult to solve by directly sampling the entire design space. Only a small region in the design space could be mapped to 1.20471 or greater in the efficiency active subspace. Therefore, an effective method was to limit the sample space to the vicinity of  $x'_{\max}$ . Each design parameter was selected from a region centered on  $x'_{\max}$  in the design space. The length of the region in each dimension was set to be 10% of the length of the design space.

Lastly, a total of thirty sets of unknowns were sampled using average random sampling, and by solving Equation (17), 30 optimized fan designs were produced. The aero-thermal performances of these designs were then calculated using the *Multall* solver, and the results are shown in Figure 13. Figure 13(a) shows that the adiabatic efficiency of the optimized fans was, on average, higher than that of the baseline design, but it did not reach the highest theoretical efficiency. Some issues with the fitting curves may need to be addressed to improve efficiency further. Figure 13(b) indicates that the mass flow of the optimized fans was slightly different from the base mass flow, but it centered around 90.656. Based on this result, the authors proposed changing the aimed mass flow from 92.022 to 93.388, as mass flow has a strong linear changing tendency. On the other hand, the pressure ratios of the optimized fans remained largely unchanged compared to those of the base fan, as shown in Figure 13(c). To correct the target value of the indefinite equation, the authors first noticed that the scatter

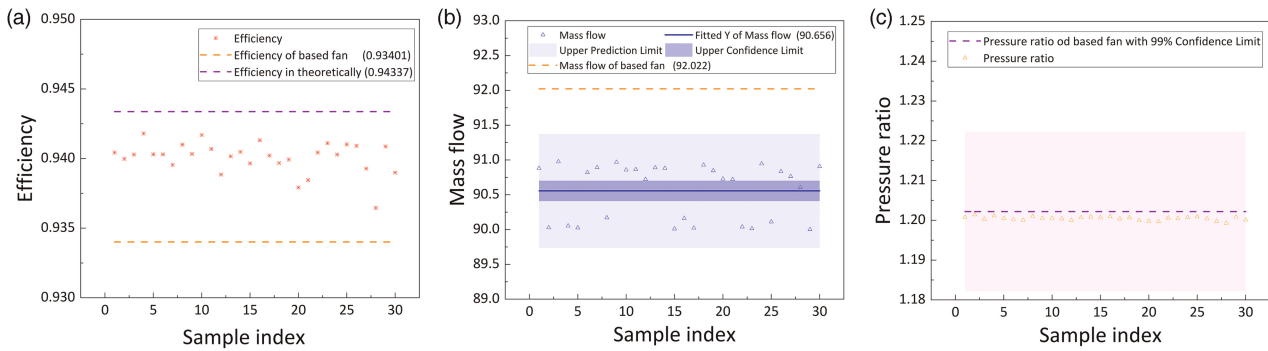


Figure 13. Aero-thermal performance of 20 optimized fans: adiabatic efficiency (a), mass flow (b) and pressure ratio (c).

distribution on the horizontal axis in Figure 11(a) was limited below 0.8, which made the fitting curve heavily dependent on the data below 0.8 and imprecise at the largest value point. To address this issue, the authors set groups of random aimed values above 0.8 of  $M_{1x}$  in Equation (17) and regenerated the fitting curve with new samples. Then, the aimed value of mass flow in Equation (14) was set to 93.388, and new fan designs were reproduced.

After implementing the corrections discussed above, Figure 14(a) plots the fitting curve of the efficiency, which was generated using 200 new special samples, and an excellent result was obtained, as seen in Figure 14(b), where the mass flow was around the base value of 92.022 with a 95% confidence limit zone. The fitting function is described in Equation (18).

$$f'_1 = 0.937 + 0.0117z_1 - 0.007z_1^2 \tag{18}$$

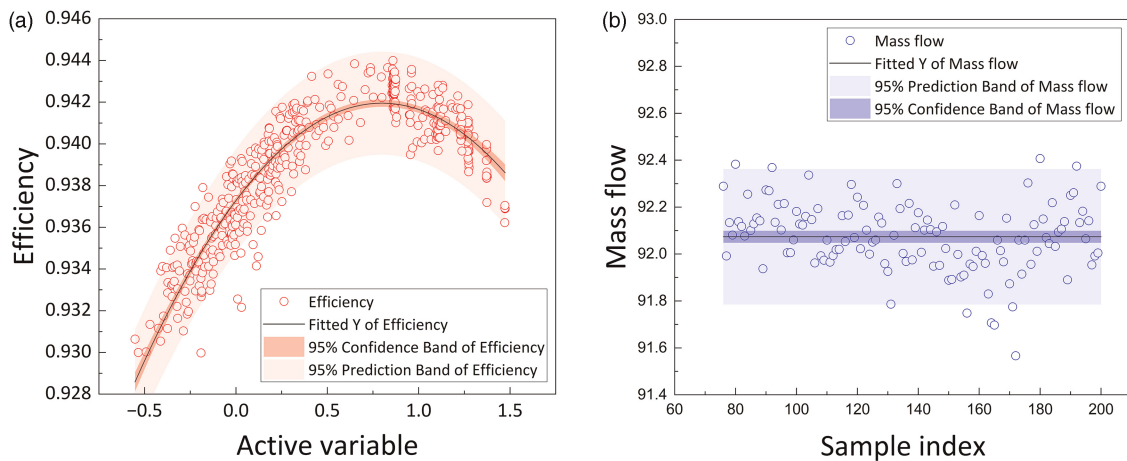


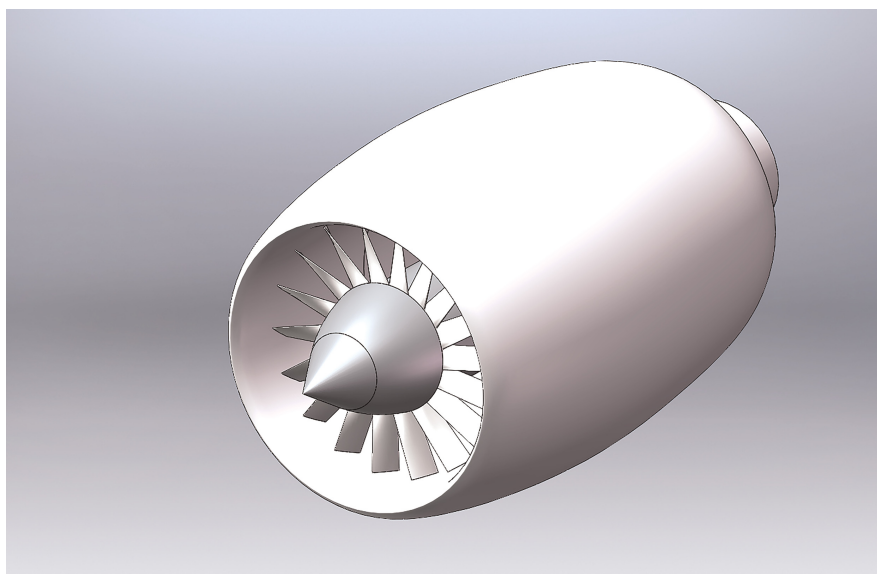
Figure 14. The corrected results: adiabatic efficiency (a) and mass flow (b).

Table 2. Aero-thermal performance of the optimized fan designs.

Fan index	1	2	3	4	5	6	7	8	9	10
Adiabatic efficiency	0.944	0.944	0.942	0.943	0.943	0.943	0.943	0.943	0.943	0.943
Mass flow (kg/s)	92.164	92.166	92.07	92.023	91.976	91.966	92.132	92.107	92.065	92.009
Pressure ratio	1.203	1.202	12.02	1.201	1.201	1.202	1.201	1.202	1.202	1.202

**Table 3. Design choices for the optimized fan blade.**

Design Parameter	Value	Unit
Reaction	0.651	—
Flow coefficient	0.811	—
Loading coefficient	0.581	—
Radius	0.337	m
Blade axial chord 1st row	0.112	m
Blade axial chord 2nd row	0.090	m
Row gap	0.215	chord
Stage gap	0.540	chord
First row deviation angle	5.222	deg
Second row deviation angle	3.949	deg
First row incidence angle	-2.781	deg
Second row incidence angle	-2.618	deg
First row LE QO angle	84.625	deg
First row TE QO angle	95.568	deg
Second row LE QO angle	94.822	deg
Second row TE QO angle	84.494	deg



**Figure 15. 3D model of the optimized ducted fan with 18 rotors and 4 stators.**

The best value point of this function was found to be 0.82, which corresponded to the highest efficiency of 94.21%. As a result, the value of 0.82 was set as the final aimed value of  $M_{1x}$  in Equation (17), along with the desired value of the mass flow, to solve the indefinite equation group using the abovementioned method. The results of the optimized fan after adjusting the aim value are presented in Table 2.

Finally, the blade design with the highest efficiency was chosen as the optimal design, with an adiabatic efficiency of 0.944, mass flow of 92.164, and pressure ratio of 1.203. The primary parameters of the optimized fan are presented in Table 3. Additionally, the blade shape parameters obtained from the optimization process are used to generate a profile file by recalling a customized *Multall* solver, which includes the 3D coordinates of the stator and rotor. *Matlab* codes are then used to convert the profile file into a format that can be used in *Solidworks* software. The resulting 3D model of the optimized ducted fan is presented in Figure 15.

## Conclusions

The preliminary design of turbomachinery aerodynamics traditionally relies heavily on the engineer's experience, which can be a time-consuming and inaccurate process. To address this challenge, this paper proposes a novel optimization strategy for turbomachinery aerodynamic preliminary design using active subspace. The method utilizes active subspace techniques to reduce the dimensionality of the design space, making efficient and accurate exploration of the space possible. The proposed method was applied to a single-stage fan, where the goal was to optimize the adiabatic efficiency while keeping the mass flow and pressure ratio constant. The following key findings were highlighted:

1. The active subspace optimization method is robust and efficient, requiring minimal trial cost to quickly optimize the aerodynamic design of the single-stage fan blade.
2. The active subspace can be calculated independently of the training sample calculation process.
3. The active subspace represents the primary direction in which the objective changes the most, while the orthogonal direction remains steady, allowing for efficient optimization in a low-dimensional space.

To conclude, the proposed methodology presents a promising approach for accurate and rapid optimization of turbomachinery aerodynamics design. However, this approach has some limitations, including the fitting curve's dependence on data and possible errors. Further exploration of optimization design methods remains critical for preliminary design.

## Nomenclature

$\hat{x}_j$	the vector of blade parameters for the $j$ th training sample
$x_l$	the vector of the lower boundary for design space
$x_u$	the vector of the upper boundary for design space
$\mu$	the vector of standard deviation in Gaussian random sampling
$\sigma$	the vector of average in Gaussian random sampling
$x_j$	the vector of normalized $\hat{x}_j$
$z_j$	the forward map of $x_j$ in active subspace

## Funding sources

The authors would like to acknowledge the support from National Science and Technology Major Project (J2019-I-0007-0007).

## Competing interests

Xu Jiasen declares that he has no conflict of interest. Lou Fangyuan declares that he has no conflict of interest.

## References

- Cho C. H., Cho S. Y., Ahn K. Y., and Kim Y. C. (2009). Study of an axial-type fan design technique using an optimization method. *Proceedings of the Institution of Mechanical Engineers, Part E: Journal of Process Mechanical Engineering*. 223 (3): 101–111. <https://doi.org/10.1243/09544089JPME254>.
- Constantine P. G. (2015). *Active Subspaces: Emerging Ideas for Dimension Reduction in Parameter Studies*. Philadelphia: Society for Industrial and Applied Mathematics.

- Danieli P., Masi M., Delibra G., Corsini A., and Lazzaretto A. (2021). Assessment of MULTALL as CFD code for the analysis of tube-axial fans. *Journal of Turbomachinery*. 143 (7): 1–10. <https://doi.org/10.1115/1.4050445>.
- Denton J. D. (2017). Multall: an open source, computational fluid dynamics based, Turbomachinery Design System. *Journal of Turbomachinery*. 139 (12): 1–14. <https://doi.org/10.1115/1.4037819>.
- Kim, H.D., Perry, A.T., and Ansell, P.J. (2018). A review of distributed electric propulsion concepts for air vehicle technology. In 2018 AIAA/IEEE Electric Aircraft Technologies Symposium, pp. 1–21.
- Li J. and Gao Z. (2005). Analysis of Aerodynamic Characteristics of Ducted Fan. *Journal of Nanjing University of Aeronautics and Astronautics*. 2005 (6): 680–684.
- Perry, A.T., Ansell, P.J., and Kerho, M. (2018). Aero-propulsive and propulsor cross-coupling effects on a distributed propulsion system. In 2018 AIAA Aerospace Sciences Meeting, 55 (6), pp. 2414–2426.
- Scillitoe, A.D., Ubald, B., Seshadri, P., and Shahpar, S. (2020). Design space exploration of stagnation temperature probes via dimension reduction. In Proceedings of the ASME Turbo Expo 2020: Turbomachinery Technical Conference and Exposition, 2C, pp. 1–12.
- Seshadri P., Shahpar S., Constantine P., Parks G., and Adams M. (2018). Turbomachinery active subspace performance maps. *Journal of Turbomachinery*. 140 (4): 1–11. <https://doi.org/10.1115/1.4038839>.
- Wang N., Xie Q., Su X., and Ren Z. (2020). Quantification of modeling uncertainties in turbulent flames through successive dimension reduction. *Combustion and Flame*. 222: 476–489. <https://doi.org/10.1016/j.combustflame.2020.09.015>.
- Wang N., Yang T., and Ren Z. (2021). Active subspace variation and modeling uncertainty in a supersonic flame simulation. *AIAA Journal*. 59 (5): 1798–1807. <https://doi.org/10.2514/1.J059977>.
- Wei J., An J., Zhang Q., Zhou H., and Ren Z. (2023). Exploiting active subspaces for geometric optimization of cavity-stabilized supersonic flames. *AIAA Journal*. 61 (8): 3353–3364.
- Turner M. G., Merchant A., and Bruna D. (2010). A turbomachinery design tool for teaching design concepts for axial-flow fans, compressors, and turbines. *Journal of Turbomachinery*. 133 (3): 1–12.
- Wick, A.T., Hooker, J.R., and Zeune, C.H. (2015). Integrated aerodynamic benefits of distributed propulsion. In 53rd AIAA Aerospace Sciences Meeting.
- Yang F., Fang Z., and Xiang S. (2021). Technology innovation and practice of electric aircraft in China. *Acta Aeronautics Sinica*. 43 (3): 7–12.